Solid State Sciences 13 (2011) 95–100

Contents lists available at ScienceDirect

Solid State Sciences

journal homepage: www.elsevier.com/locate/ssscie

Surface characterization of Ti-Si-C-ON coatings for orthopedic devices: XPS and Raman spectroscopy

Cristina Oliveira [a], R. Escobar Galindo [b,c], C. Palacio [d], S. Calderon V [a,*], B.G. Almeida [a], M. Henriques [e], A. Espinosa [d], S. Carvalho [a]

[a] Centro de Física, Universidade do Minho, Campus de Azurém, 4800-058 Guimarães, Portugal
[b] Centro de Microanálisis de Materiales, Universidad Autónoma de Madrid, Cantoblanco, 28049, Spain
[c] Instituto de Ciencia de Materiales de Madrid (ICMM -CSIC), Cantoblanco, 28049, Madrid, Spain
[d] Departamento de Física Aplicada (CXII), Universidad Autónoma de Madrid, Cantoblanco, 28049, Spain
[e] IBB-Institute for Biotechnology and Bioengineering Centre for Biological Engineering, Universidade do Minho Campus de Gualtar, 4700-057, Portugal

ARTICLE INFO

Article history:
Received 16 July 2010
Received in revised form
10 October 2010
Accepted 25 October 2010
Available online 30 October 2010

Keywords:
Sputtering
GDOES
Raman
XPS

ABSTRACT

Ti–Si–C–ON films were deposited by DC reactive magnetron sputtering and their chemical properties, biofilm formation and toxicity were characterized. Based on the films composition three different growth regimes were identified on the films; (I) N/Ti = 2.11 (high atomic ratio) and low oxygen content; (II) 0.77 ≤ N/Ti ≤ 1.86 (intermediate atomic ratio) and (III) N/Ti ≤ 0.12 (low ratio) and high oxygen content. The phase composition varied from mainly TiN on regime I to TiCN on regime 2 and titanium oxides on regime III. Taking into account the results of biological characterization (biofilm formation and cytotoxicity), it was possible to conclude that samples with a high TiN content (regime I) presented more favorable biocompatibility, since it was less prone to microbial colonization and also displayed a low cytotoxicity.

1. Introduction

In recent years, strong efforts have been made on the development of new coatings for orthopedic implants, in order to improve their tribological properties as well as their biocompatibility. The aim has been guided towards reducing failures due to overloading, fatigue, wear, corrosion and infection [1,2]. Titanium nitride (TiN), for instance, has been used for biomedical applications. However, it presents a high friction coefficient and a relatively high wear rate [3], leading to an increased risk of failing. Furthermore, it has been demonstrated that the incorporation of silicon in the TiN based structure increase the hardness of the films [4–6], but the friction coefficient is not improved. Hence, studies have been focused on Ti-Si-C-N and have shown that the friction coefficients for high carbon concentrations are lower, due to the formation of a graphite-like lubricating phase [7]. Consequently, Changa [8] demonstrated that the microstructure of coatings transformed from Ti–Si–C–N to TiSi containing diamond-like carbon films structure strongly depending on the carbon content. Also the Si addition into Ti–C–N films not only increase the hardness, but an amorphous phase of SiCxNy mixed with the Ti(C,N) appeared, depending on the carbon content in the coatings [7,9–11].

In addition, previous work carried out by this group on Ti–Si–C–ON coatings showed that the oxygen (O) content and N/Ti ratio have a competitive role on the film properties [12]. Moreover, it is expected that adding small amounts of oxygen to these carbides/nitrides, some structural changes will occur, offering the possibility to taylor the material to a much wider set of desired properties. On the other hand, it is reported that high oxygen content could lead to low hardness of the films [8]. Nevertheless, the influence of oxygen on the structure of the quaternary compound Ti-Si-C-N is not well established yet.

Despite the results already obtained, there is still a lack in the knowledge of the structural arrangements of these coatings. Hence, this paper reports the chemical bonding information obtained by Raman and X-ray Photoelectron Spectroscopy (XPS). Since the biological properties are important to investigate the feasibility of these Ti–Si–C–ON coatings for orthopedic applications, additional biological results are also presented.

2. Experimental details

The Ti–Si–C–ON samples were deposited by d.c. reactive magnetron sputtering from two opposed high purity (99.6%) Ti

* Corresponding author.
E-mail address: secave44@gmail.com (S. Calderon V).

1293-2558/$ – see front matter © 2010 Elsevier Masson SAS. All rights reserved.
doi:10.1016/j.solidstatesciences.2010.10.015

targets (20×10 cm^2): one Ti target with incrusted Si pellets (hereafter designated as TiSi target) and the other with carbon pellets (designated as TiC target), placed in the preferential eroded zone. The area occupied by the pellets was close to 11 cm^2 in each target. Depositions were carried out under an Ar + ($N_2 + O_2$) atmosphere on an Alcatel SCM 650 sputtering system. The base pressure in the chamber was about 10^{-4} Pa and rose to 4×10^{-1} Pa during the depositions. The coatings were deposited on 316L stainless steel (medical grade steel) and on single crystal silicon (100) substrates for further structural analysis. During the depositions, the substrates were rotated 70 mm above the target at a constant speed of 7 rpm to assure a homogenous deposition of the films.

In order to change the oxygen content, samples were grown using different $N_2 + O_2$ flow rates (ranging N_2 from 6.5 to 0 sccm and O_2 from 0 to 5.25 sccm), while maintaining an Ar flow constant at 60 sccm. The substrate bias voltage and the temperature were kept constant at −50 V and 200 °C, respectively. The current density applied to the TiC target was 5 mA/cm^2 and to the TiSi target was 6 mA/cm^2. The detailed information about the deposition parameters is presented on Table 1.

The stoichiometry of the films was investigated by means of Rutherford Backscattering Spectrometry (RBS) and Glow Discharge Optical Emission Spectroscopy (GDOES). RBS experiments were performed with a 5 MV HVEE Tandetron [13]. RBS spectra were collected using 2 MeV H^+ ions at an ion dose of 7 μC. Data acquisition was performed simultaneously using two silicon surface barrier detectors located at scattering angles of 170° and 135°, respectively, and with an energy resolution of 15 keV. The experimental spectra were fitted with the program RBX [14]. GDOES was carried out using a Jobin Yvon RF GD Profiler equipped with a 4 mm diameter anode and operating at a typical radio frequency discharge pressure of 650 Pa and power of 40 W. The setup was calibrated using standard materials of known composition. In order to improve the quantification of nitrogen, a series of chromium nitride coatings, deposited by magnetron sputtering, were used as calibration samples [15].

Chemical bonding information was obtained by Raman and X-ray Photoelectron Spectroscopy (XPS). The Raman spectra were acquired with a Jobin-Yvon HR 460 monochromator and a nitrogen cooled CCD. The excitation light was the 514.5 nm line of an Ar-Kr laser. The incident and scattered beams were focused using an Olympus microscope and a Kaiser Super-Notch filter was used to suppress the elastic scattered light. The XPS spectra were measured using a hemispherical analyzer (SPECS Phoibos 100 MCD-5). The pass energy was 9 eV giving a constant resolution of 0.9 eV. The Au $4f_{7/2}$, Ag $3d_{5/2}$ and Cu $2p_{3/2}$ lines of standard samples at 84.0, 368.3 and 932.7 eV, respectively, were used in order to calibrate binding energies. A twin anode (Mg and Al) X-ray source was operated at a constant power of 300 W using Mg Kα radiation. The samples were sputter-cleaned in situ using a broad 3 keV Ar^+ beam, for 10 min.

For the biological studies (biofilm formation and cytotoxicity) one sample per each regime was assayed, namely samples with N/Ti of 0.04, 0.77 and 2.11. Biofilms of *Staphylococcus epidermidis* were formed, in Tryptic Soy Broth, on coated materials for 48 h, at 120 rpm and 37 °C. Total biomass was determined by staining samples with crystal violet (Abs CV) and by absorbance reading at 570 nm [16]. At least three replicates were performed in three different assays. Cytotoxicity was determined using a fibroblast 3T3 cell line. Coupons of sample materials were placed in indirect contact (an inert plastic holder was used) with confluent cells, for 24 h at 37 °C and 5% CO_2 in 1 ml of Dulbecco's Modified Eagle Medium (supplemented with 10% of fetal bovine serum) and the controls were performed in the absence of coupons. Cellular activity was determined using MTS (3-(4,5-dimethylthiazol-2-yl)-5-(3-carboxymethoxyphenyl)-2-(4-sulfophenyl)-2H-tetrazolium, inner salt - Promega CellTiter 96® AQ_{ueous} Non-Radioactive Cell Proliferation Assay). The percentage of cell death was determined in relation to the control, which was considered 100% of cellular activity. Again, three replicates were performed in, at least, three different assays.

3. Results and discussion

3.1. Chemical composition

The atomic composition of the samples deposited on silicon substrates, determined by RBS and GDOES, is given in Table 1. It should be pointed out that the results of the chemical composition of the films deposited on the 316L steel, obtained by these two techniques, do not show significant differences from the ones of Table 1. The values of an average of the RBS and GDOES analyses, as a function of the oxygen partial pressure and the nitrogen partial pressure ratio (p_{O2}/p_{N2}), are also shown in Table 1. The N/Ti atomic ratio tends to decrease with increasing p_{O2}/p_{N2} and the oxygen content shows an opposite behavior. Taking into account the different elemental compositions, 3 different regimes, based on the samples concentrations, can be observed: (I) N/Ti = 2.11 (high atomic ratio) and low oxygen content; (II) $0.77 \leq$ N/Ti ≤ 1.86 (intermediate atomic ratio) and (III) N/Ti ≤ 0.12 (low ratio) and high oxygen content. The chemical composition of the films as a function of deposition process parameters (p_{O2}/p_{N2}) and these different regimes are in agreement with results already published [12]. As such, we will use here the referred regimes, for consistency with the previously reported results.

In Fig. 1 GDOES depth profiles are shown for coatings belonging to regime I (Fig. 1a) and III (Fig. 1b), deposited on steel substrates. Despite some carbon and oxygen contamination in the near surface, the elemental composition (Ti, Si, C, O and N) of the films, along their depth, is homogeneous, for both regimes. For the sample in regime I, the intermediate adhesive titanium-silicon layer is clearly observed.

3.2. X-ray diffraction results

Previously, the X-ray diffraction (XRD) results for these samples were already presented and discussed [12]. Nevertheless, for the sake of clarity some features should be pointed out. The XRD patterns from the samples within regime I, (high N/Ti atomic ratio)

Table 1
Overview on the chemical composition, and some deposition parameters.

Ratio N/Ti	ϕO_2 sccm	ϕN_2 sccm	Deposition rate μm/h	Working pressure Pa	pO2/pN2	Chemical Compositiom				
						Ti (at.%)	Si (at%)	C (at%)	O (at%)	N (at%)
2.11	0	6.5	0.9	0.41	0.046	26	10.1	6.3	2.8	54.8
1.86	1.005	5.6	1.1	0.47	0.56	26.3	7.5	2.9	14.5	48.8
0.77	0.825	2.5	1.2	0.43	0.8	40.8	7.2	9.4	11	31.6
0.12	0.825	1	1.5	0.48	1.76	58	7.8	9.8	17.4	7
0.04	5.250	0	1.6	0.44	20	54.5	4.7	3.5	34.8	2.5

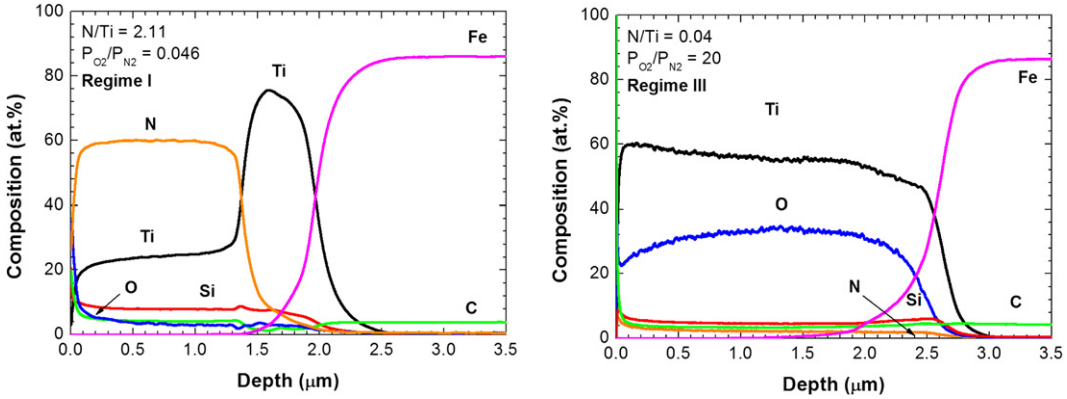

Fig. 1. GDOES depth profiles for Ti–Si–C–ON coatings belonging to (left) regime I: N/Ti = 2.11 p_{O2}/p_{N2} = 0.046 and (right) regime III: N/Ti = 0.04 p_{O2}/p_{N2} = 20.

and low oxygen content exhibit reflections that correspond to a mixture of two different phases: a metallic-like Ti and an fcc TiN type structure. For regime (II) 0.77 ≤ N/Ti ≤ 1.86 (intermediate atomic ratio), the films crystallize also in a B1-NaCl crystal structure typical for $TiC_{0.2}N_{0.8}$. For regime III–N/Ti ≤ 0.12 (low ratio) and high oxygen content, the films exhibit a polycrystalline structure, due to the increase of the oxygen concentration. The increasing concentration of N-vacancies (decreasing N/Ti) can progressively be filled by oxygen atoms, forming Ti-O phases. These different regimes and the corresponding phases were obtained for films deposited on both substrates.

3.3. Raman and XPS analysis

The structural and chemical properties of the Ti–Si–C–ON films were probed by means of Raman and XPS studies. Fig. 2 shows the Raman spectra of Ti–Si–C–ON samples deposited on silicon, with different p_{O2}/p_{N2} (and consequently different regimes for the N/Ti atomic ratio). The absence of sharp and well-defined peaks suggests local structural disorder of the prepared films. In a perfect crystal with fcc structure (as in TiN) every ion is at a site of inversion symmetry and consequently first-order Raman scattering is forbidden [17]. However, Physical Vapor Deposition (PVD) coatings are known to contain defects in the crystalline lattice reducing the effective symmetry and giving rise to defect-induced Raman spectra, as in the films studied. Fig. 3 shows the Ti2p, Si2p, C1s, O1s and N1s core level XPS spectra of the deposited Ti–Si–C–ON films.

For the film with N/Ti = 2.11(regime I), two weak and broad bands in the Raman spectra, centered at about 300 and 550 cm^{-1} are observed. According to Constable et al. [17] these bands can be associated to longitudinal/transversal acoustic (LA/TA) and optical (LO/TO) vibrational modes of Ti-N. These modes are consistent with the dominant presence of TiN in the XRD results [12], for this compositional region. On the XPS analysis, the Ti2p spectra (Fig. 3a), can be simulated with a doublet (Ti2p3/2 and Ti2p1/2 separated by 5.8 eV) attributed to the electron binding energies of TiN(455 and 460.8 eV, respectively), according to the literature [5,18–20]. However, due to the peak asymmetry observed in the spectrum, a small contribution of Ti-C bonds (454.5 eV and 460.3 eV) cannot be discarded. In order to quantify separately the individual contribution of those two phases a complete deconvolution of the spectra should be performed. In fact, the binding energies for titanium are consistent with the C-Ti and N-Ti bonds observed at the C1s (282 eV) and N1s (397 eV) on the XPS spectra of Fig. 3c and e, respectively [21]. For this same regime, the Si2p XPS spectrum (Fig. 3b) shows a major contribution centered at 101.4 eV, attributed to Si–C–N bonds [22,23]. Shalaeva et al. [23] stated that for Ti-Si-N-O films a silicon content of 10 at % induced a nearly nanocrystalline structure of TiSiN(O) with small average grain size: 1.5–2 nm. In the present case, the presence of Si–C–N bonds in the XPS spectrum indicates that silicon is partially dissolved in the films forming a Ti-Si-(C,N) cubic solid. Within the O1s region it is observed a weak and wide peak (FHWM > 3 eV) centered at 531.2 eV. This binding energy lies between the reported values for crystal lattice O-Ti (529.6 eV) and O-Si (532.7) bonds, suggesting the formation of titanium silicates [24,25].

For regime (II) 0.77 ≤ N/Ti ≤ 1.86 (intermediate atomic ratio), both a decrease in nitrogen content and an increase in carbon content were observed. The Raman spectrum for the sample with N/Ti = 1.86 shows the same peaks as the one for the sample of regime I, but a shoulder located at around 720 cm^{-1} starts to appear. This band, also observed in CN_x films [26], can be attributed to the Ti(C,N) phase. In the XPS spectra there is a progressive decrease of the Ti-N signal (Fig. 3e) and a subsequent increase of the C-Ti bonds (Fig. 3c), which is consistent with the progressive substitution of the nitrogen by carbon, on the underlying TiN structure, to form a fcc Ti(C,N) phase. The Si2p XPS spectrum of sample with N/Ti = 1.86 shows a major contribution at 102 eV attributed to Si-N bonds [22] that can be associated to an amorphous SiN_x phase. This phase practically disappears on sample with N/Ti = 0.77 due to the decrease of nitrogen in the deposition chamber.

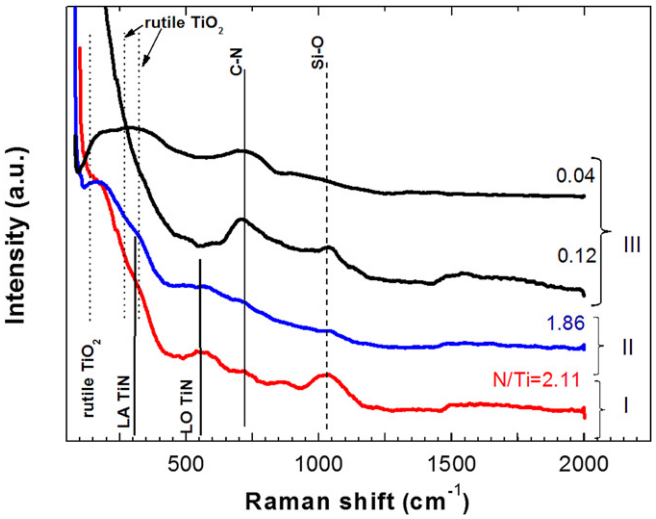

Fig. 2. Raman spectra of the Ti–Si–C–ON coatings deposited by DC reactive magnetron sputtering with different N/Ti ratios.

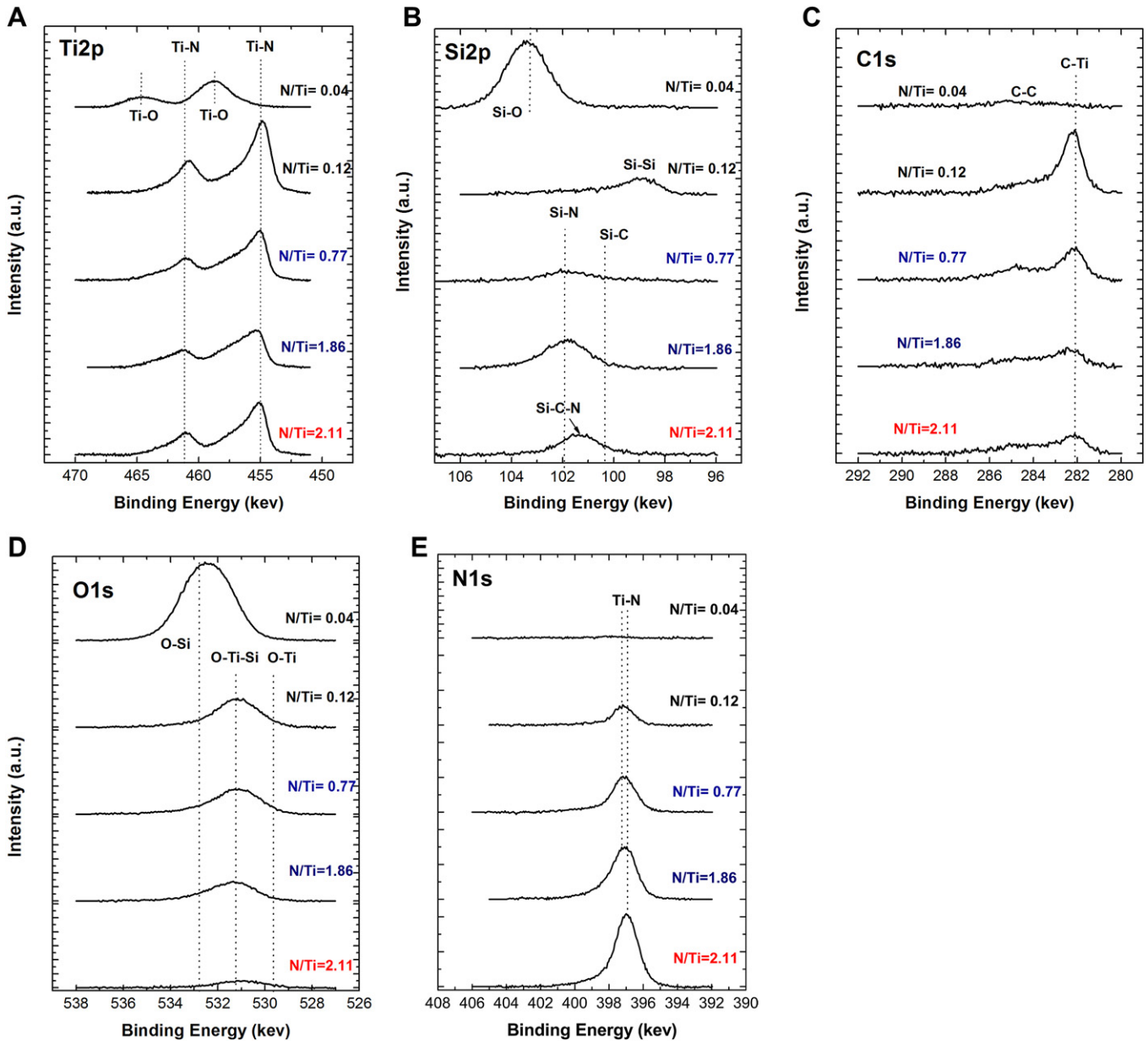

Fig. 3. XPS spectra of a) Ti2p, b) C1s, c) N1s, d) O1s and e) Si 2p core levels of the Ti–Si–C–ON coatings deposited by DC reactive magnetron sputtering, with different N/Ti ratios.

A considerable modification of the spectral shape occurs for the samples deposited with high p_{O2}/p_{N2} that induces a low N/Ti atomic ratio and high oxygen content (regime III N/Ti $\leq$ 0.12). The Raman spectrum for the sample with N/Ti = 0.12 confirms the progressive nitrogen substitution by carbon atoms to form fcc Ti (C,N) phases, since the band around 720 cm^{-1}, due to the C-N bond vibration, is clearly visible. This is supported by the shift of the Ti2p main signal towards lower binding energies (indicating the formation of a Ti–C–N phase as discussed in [24]) and the increase of the C-Ti bonds observed in the XPS spectra of Fig. 3a and c, respectively. The Si2p spectrum only shows a small contribution of metallic silicon at 99 eV, as the amount of nitrogen present in the films (7%) is too low to form a SiNx phase in sample with N/Ti = 0.77. Finally, for the sample with higher O content (N/Ti = 0.04 atomic ratio), the Raman spectrum clearly shows the presence of bands characteristic of the rutile phase of TiO_2 [18]. It is worth noting that these bands are quite broad, due to structural disorder or stress in this phase, but also due to nanometric grain sizes present in the films. Similarly, the observed Raman band around 1030 cm^{-1} is due to the stretching Si-O vibration from SiO_x [27]. These results agree with the previous XRD and FTIR characterizations [12], since, the sample deposited with high p_{O2}/p_{N2} low N/Ti atomic ratio and high oxygen content (regime N/Ti $\leq$ 0.12), exhibits a polycrystalline structure with the formation of nano-sized clusters. The XPS Ti2p spectrum presents a doublet at 459 eV and at 464.8 eV corresponding to titanium oxide [28] bonds. Moreover, the Si2p spectrum has a distinctive peak near 103.2 eV associated to Si-O bonds [29]. This is supported by the broad peak ($>$ 2 eV) of O1s centered at 532.4 eV that can be deconvoluted into two components at 532.7 eV and 531.4 eV, respectively. The first component should be attributed to O-Si bonds and the second one suggests the formation of Ti–O–Si cross-linking bonds by analogy with similar results found during the oxidation of Ti/Al interfaces [28]. The very low nitrogen content in this sample (see Fig. 3e) confirms that the predominant phases are titanium and silicon oxides, in agreement with the Raman results.

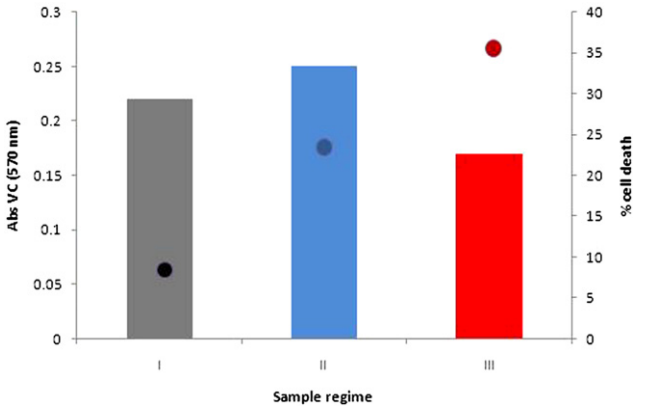

Fig. 4. Values of biofilm biomass, measured by crystal violet absorbance (bars) and cytotoxicity, quantified by the % of cell death (circles).

3.4. Biological characterization

Microbial colonization of implant devices has been one of the main causes of implant failure and this colonization is often associated with biofilm formation. In these biofilms, heterogeneous communities of microorganisms are embedded in a polymeric matrix, which confers them resistance to antimicrobial agents and allows them future detachment and colonization/infection of additional body sites. Moreover, as implants have to be in direct contact with the human body they must be biocompatible, meaning that they cannot cause human tissue cell death. Here, the biological characterization, which includes the determination of biofilm formation and cytotoxicity of the films, was performed with one representative sample from each regime (Fig. 4).

From Fig. 4 it is possible to observe that all assayed samples were prone to microbial colonization. Previously, it was shown that the sample with low N/Ti atomic ratio and high oxygen content (regime III) presented a lower biomass amount than the samples from the two other regimes (which presented similar values among them) due to the formation of titanium oxide rich surfaces that are less prone to colonization. Similar results were also described by other authors [30,31] enhancing the microbial colonization inhibition of titanium dioxide surfaces, even for other applications. However, its cytotoxicity analysis revealed a high value of cellular death, hindering its selection as biomaterial. In fact, both properties should always be assessed because a biomaterial surface must resist biofilm formation as well as presenting low cytotoxicity.

Regarding the cytotoxicity results here presented (circles on Fig. 4) it is possible to verify that the percentage of cell death varies according to the regime of samples preparation. The sample from regime I showed lower cytotoxicity than the samples from the other regimen. That sample is characterized by a TiN structure, in opposition to the sample with a composition more similar to TiO_2 (regime III), which presented a higher value of cytotoxicity.

Thus, aiming at determining which coating preparation conditions lead to the best biological properties, it is possible to verify that, from all the samples assayed, the film with N/Ti = 2.11, from regime I presented the best compromise (lowest cytotoxicity and a moderate microbial colonization).

4. Conclusions

Ti–Si–C–ON thin films have been prepared by unbalanced d.c. magnetron sputtering with different p_{O2}/p_{N2}. Their structural and chemical properties were characterized, by Raman and XPS spectroscopies, and correlated with their biofilm formation and cytotoxicity.

From the Raman and XPS analysis, 3 different composition regimes were observed: (I) N/Ti = 2.11 (high atomic ratio) and low oxygen content; (II) $0.77 \leq N/Ti \leq 1.86$ (intermediate atomic ratio) and (III) $N/Ti \leq 0.12$ (low ratio) and high oxygen content. The film composition varied from TiN within the regime I (N/Ti = 2.11), to TiCN within the regime II ($0.77 \leq N/Ti \leq 1.86$), towards titanium oxide on regime III ($N/Ti \leq 0.12$).

From the analysis of the biological properties it can be ascertained that there was biofilm formation on all samples and that they all presented low cytotoxicity. However, samples from regime I (high N/Ti ratio) presented moderate biofilm formation and low cytotoxicity.

In conclusion, this work puts on evidence that using different parameters during the coating process leads to different regimes ranging from TiO_2 to TiN, and that the latter represents the best choice for the coating of biomaterials, since it presents the best compromise between biological properties (lowest cytotoxicity and low microbial colonization).

Acknowledgments

The authors are grateful to Dr. Alicia Andrés, Instituto de Ciencia de Materiales de Madrid (ICMM-CSIC), for his assistance in carrying out the Raman spectroscopic analysis. The work was financially supported by the CRUP Institution (project "Acção N° E-1007/08), and the Spanish Ministry of Science and Innovation (projects FUNCOAT CSD2008-00023, MAT2008-06618-C02 and Integrated action HP016-2007). This research is partially sponsored by FEDER funds through the program COMPETE- Programa Operacional Factores de Competitividade and by Portuguese national funds through FCT-Fundação para a Ciência e a Tecnologia, under the project PTDC/CTM/102853/2008.

References

[1] R.O. Darouiche, G. Green, M.D. Mansouri, Int. J. Antimicrob.Agents 10 (1998) 83.
[2] U.K. Mudali, T.M. Sridhar, B. Raj, Sadhana 28 (2003) 601.
[3] S. Piscanec, L.C. Ciacchi, E. Vesselli, G. Comelli, O. Sbaizero, S. Mariani, et al., Acta Mater. 52 (2004) 1237.
[4] R.F. Zhang, S. Veprēk, Thin Solid Films 516 (2008) 2264.
[5] L. Rebouta, C.J. Tavares, R. Aimo, Z. Wang, K. Pischow, E. Alves, T.T. Rojas, J.A. Odriozola, Surf. Coat. Technol. 133-134 (2000) 234.
[6] F. Vaz, L. Rebouta, P. Goudeau, J. Pacaud, H. Garem, J.P. Rivière, A. Cavaleiro, E. Alves, Surf. Coat Technol. 133-134 (2000) 307.
[7] S.L. Ma, D.Y. Ma, Y. Guo, B. Xu, G.Z. Wu, K.W. Xu, P.K. Chu, Acta Mater. 55 (2007) 6350.
[8] C. Chang, T. Hsieh, J. Mater. Process. Tech. 209 (2009) 5521.
[9] S. Abraham, E.Y. Choi, N. Kang, K.H. Kwang, Surf. Coat Technol. 202 (2007) 915.
[10] R. Wei, Surf. Coat Technol. 203 (2008) 538.
[11] H. Lin, J. Duh, R. Wei, C. Rincon. J. Lee. Surf. Coat, Technol. doi:10.1016/j.surfcoat.2010.07.070.
[12] C. Oliveira, L. Gonçalves, B.G. Almeida, C.J. Tavares, S. Carvalho, F. Vaz, R. Escobar Galindo, M. Henriques, M. Susano, R. Oliveira, Surf. Coat Technol. 203 (2008) 490.
[13] A. Climent-Font, F. Pászti, G. García, M.T. Fernández-Jiménez, F. Agulló, Nucl. Instr. and Meth. Phys. Res. B. 219-220 (2004) 400.
[14] E. Kotai, Nucl. Instrum. Methods Phys. Res. Sect. B. B85 (1994) 588.
[15] R. Escobar Galindo, E. Forniés, R. Gago, J.M. Albella, J. Anal. Spectrom. 22 (2007) 1512.
[16] M. Henriques, J. Azeredo, R. Oliveira, J. Biomed. Sci. 63 (2006) 5.
[17] C.P. Constable, J. Yarwood, W.D. Münz, Surf. Coat. Technol. 116-119 (1999) 155.
[18] D. Pilloud, J.F. Pierson, M.C. Lucas, A. Cavaleiro, Surf. Coat. Technol. 202 (2008) 2413.
[19] X. Song, D. Gopireddy, C.G. Takoudis, Thin Solid Films 516 (2008) 6330.
[20] A. Vyas, K.Y. Li, Z.F. Zhou, Y.G. Shen, Surf. Coat. Technol. 200 (2005) 2293.
[21] J. Alami, P. Eklund, J. Emmerlich, O. Wilhelmsson, U. Jansson, H. Högberg, et al., Thin Solid Films 515 (2006) 1731.
[22] B. Mitu, G. Dinescu, M. Dinescu, A. Ferrari, M. Balucani, G. Lamedica, et al., Thin Solid Films 383 (2001) 230.
[23] E.V. Shalaeva, S.V. Borisov, O.F. Denisov, M.V. Kuznetsov, Thin Solid Films 339 (1999) 129.

[24] C. Oliveira, R. Escobar Galindo, C. Palacio, L. Vazquez, A. Espinosa, B.G. Almeida, M. Henriques, S. Calderón, S. Carvalho, Thin Solid Films 518 (2010) 5694.
[25] L. Zhao, M. Han, J. Lian, Thin Solid Films 516 (2008) 3394.
[26] E.J. Liang, J.W. Zhang, J. Leme, C. Moura, L. Cunha, Thin Solid Films 469-470 (2004) 410.
[27] B.T. Poe, C. Romano, G. Henderson, J. Non-Cryst. Solids 241 (2004) 162.
[28] C.L. Liang, G.A. Cheng, R.T. Zheng, H.P. Liu, J.C. Li, H.F. Zhang, et al., Surf. Coat. Technol. 201 (2007) 5537.
[29] G. He, M. Liu, L.Q. Zhu, M. Chang, Q. Fang, L.D. Zhang, Surf. Sci. 575 (2005) 67.
[30] C.L. Cheng, D.S. Sun, W.C. Chu, Y.H. Tseng, H.C. Ho, J.B. Wang, P.H. Chung, J.H. Chen, P.J. Tsai, N.T. Lin, M.S. Yu, H.H. Chang, J. Biomed. Sci. 16 (2009) 7.
[31] W. Kangwansupamonkon, V. Lauruengtana, S. Surassmo, U. Ruktanonchai, Nanomedicine 5 (2009) 240.